Front. Earth Sci. 2018, 12(4): 672–682
https://doi.org/10.1007/s11707-018-0691-2

RESEARCH ARTICLE

Uncertainty in solid precipitation and snow depth prediction for Siberia using the Noah and Noah-MP land surface models

Kazuyoshi SUZUKI (✉)[1], Milija ZUPANSKI[2]

1 Institute of Arctic Climate and Environment Change Research (IACE), Japan Agency for Marine-Earth Science and Technology (JAMSTEC), Yokohama 236-0001, Japan
2 Cooperative Institute for Research in the Atmosphere, Colorado State University, Fort Collins, CO 80523-1375, USA

Abstract In this study, we investigate the uncertainties associated with land surface processes in an ensemble predication context. Specifically, we compare the uncertainties produced by a coupled atmosphere–land modeling system with two different land surface models, the Noah-MP land surface model (LSM) and the Noah LSM, by using the Maximum Likelihood Ensemble Filter (MLEF) data assimilation system as a platform for ensemble prediction. We carried out 24-hour prediction simulations in Siberia with 32 ensemble members beginning at 00:00 UTC on 5 March 2013. We then compared the model prediction uncertainty of snow depth and solid precipitation with observation-based research products and evaluated the standard deviation of the ensemble spread. The prediction skill and ensemble spread exhibited high positive correlation for both LSMs, indicating a realistic uncertainty estimation. The inclusion of a multiple snow-layer model in the Noah-MP LSM was beneficial for reducing the uncertainties of snow depth and snow depth change compared to the Noah LSM, but the uncertainty in daily solid precipitation showed minimal difference between the two LSMs. The impact of LSM choice in reducing temperature uncertainty was limited to surface layers of the atmosphere. In summary, we found that the more sophisticated Noah-MP LSM reduces uncertainties associated with land surface processes compared to the Noah LSM. Thus, using prediction models with improved skill implies improved predictability and greater certainty of prediction.

Keywords ensemble simulation, land-atmosphere interaction, ensemble spread, vertical temperature, snow prediction

Received May 26, 2017; accepted November 23, 2017

E-mail: skazu@jamstec.go.jp

1 Introduction

Land–atmosphere interactions and land surface models (LSMs) are important for understanding future climate change (Yu et al., 2016) and for demonstrating the importance of improving the parameterization of snow and soil processes. In terms of land surface schemes in regional climate models, Zeng et al. (2015) showed that land surface schemes affect heat wave prediction in China, whereas Jin et al. (2010) examined the sensitivity of LSMs in a regional climate model and concluded that sophisticated LSMs reduce the errors related to surface air temperature. In addition, land surface processes and land use changes strongly affect snow distribution and radiation balances in snowy regions (Suzuki et al., 2011, 2015a).

In the Siberian region, snow and land surface processes have significant effects on water and carbon dynamics (Suzuki et al., 2006a, 2006b). Suzuki et al. (2015b, 2016) showed that solid precipitation and evapotranspiration are important for understanding the hydrological cycle in the Lena river basin. Recently, Suzuki et al. (2017) analyzed how LSMs affect coupled atmosphere–land processes using strongly coupled atmosphere–land data assimilation, and revealed that sophisticated LSMs can reduce the uncertainty related to surface temperature. Orth et al. (2016) indicated that a coupled land–atmosphere model using a sophisticated LSM might lead to larger errors in precipitation and temperature data, compared to use a less sophisticated LSM, and suggested that the inclusion of uncertainty in LSM parameters is important for better weather prediction. In addition, the variables resolved in the LSM parameterization, such as cloud microphysics and cumulus schemes, radiation schemes and certain land and ocean variables, and the planetary boundary layer (PBL), interact directly with other physical parameterizations in the atmospheric model. Therefore, it is important to understand how the model physics of an LSM relates to

the predictability of land and atmosphere variables.

One of the best known LSMs is the Noah LSM (Ek, 2003), which is free to use and is coupled with many numerical weather models, including the North American Mesoscale model, the Global Forecast System, and other National Centers for Environmental Prediction (NCEP) modeling systems. The recently developed Noah-MP LSM (Niu et al., 2011) is an extended version of the Noah LSM with enhanced multi-physics (MP) options designed to address critical shortcomings in the Noah LSM. These two LSMs are widely used in climate studies. Using these two LSMs, we can easily evaluate how sophisticated physics processes in LSMs affect coupled land–atmosphere model predictions and uncertainty.

In this study, we examine the effects of these two LSMs on prediction uncertainties for solid precipitation and snow depth at the beginning of March 2013 in Siberia, using a framework similar to that of Suzuki et al. (2017) but focusing on the ensemble prediction step in the data assimilation process. The primary goals of this study were two-fold: (i) to investigate the differences in solid precipitation and snow depth prediction uncertainties between the Noah and Noah-MP LSMs, and (ii) to show the effects on the uncertainty of the atmospheric state (temperature profile) in the Noah and Noah-MP LSMs.

2 Methodology

2.1 Model and prediction uncertainty

We conducted prediction uncertainty experiments using ensemble simulations with a coupled atmosphere–land surface model. The atmospheric model used in this study was the regional Weather Research and Forecasting (WRF) model- Advanced Research WRF (ARW) Version 3 (Skamarock et al., 2008). In the WRF-ARW, all model atmospheric settings are defined as in Table 1.

The Noah LSM has one canopy layer and four soil layers of thickness 0.1, 0.3, 0.6, and 1.0 m (total soil depth 2 m) located at depths of 0, 0.1, 0.4, and 1 m, respectively, from the ground surface to the bottom. The Noah LSM employs a single snow layer. The lower 1 m acts as a reservoir with gravity drainage at the bottom, and the upper 1 m of the soil serves as the root zone. The surface skin temperature is determined following Mahrt and Ek (1984) by applying a single, linearized surface energy balance equation representing the combined ground/vegetation surface. Thus, the vegetation canopy does not affect the surface energy balance directly. The Noah-MP is a version of the Noah LSM augmented with multi-physics options. The differences between these models include the following: 1) restructuring the model to include a separated vegetation canopy accounting for vegetation effects on surface energy and water balances; 2) a modified two-stream approximation scheme to include the effects of vegetation canopy gaps that vary with solar zenith angle and the effects of canopy 3-D structure on radiation transfer; and 3) a 3-layer physically based snow model. Both LSMs utilize the same vertical levels in the atmosphere and soil, and each simulates soil moisture (both liquid and frozen), soil temperature, skin temperature, snowpack depth, snowpack water equivalent, canopy water content, and the energy flux and water flux terms of the surface energy balance and surface water balance. Table 2 summarizes the differences in snow and vegetation simulations between the two LSMs.

Table 1 Schemes used in experiments for cumulus clouds, planetary boundary layer, microphysics, and longwave and shortwave radiation transfer parameterizations

Parameterization	Schemes used
Cumulus clouds	Kain–Fritsch convection scheme (Kain, 2004)
Planetary boundary layer	Yonsei University scheme (Hong et al., 2006)
Microphysics	Lin scheme (Lin et al., 1983)
Longwave radiation transfer	Rapid Radiative Transfer Model of Global climate models (Iacono et al., 2008)
Shortwave radiation transfer	(Chou and Suarez, 1999)

Prediction uncertainty is typically calculated from ensemble runs of prediction models. In our application, the land surface prediction uncertainty is produced by running ensembles of the WRF models with a land surface scheme. Specifically, we use the framework of the Maximum Likelihood Ensemble Filter (MLEF) (Zupanski, 2005) data assimilation system but without the analysis component. In general, an ensemble data assimilation system consists of (i) ensemble initiation, (ii) ensemble prediction, and (iii) analysis. We use steps (i) and (ii) but

Table 2 Description of two LSMs

Parameters	Noah LSM	Noah-MP LSM
Vegetation	One canopy layer, simple canopy resistance. Simple Jarvis-type canopy resistance function, single linearized energy balance equation representing combined ground–vegetation surface, considering seasonal LAI and green vegetation fraction	Snow interception includes loading–unloading, melt–refreeze capabilities, and sublimation of canopy-intercepted snow, along with detailed representation of transmission and attenuation of radiation through the canopy, within- and below-canopy turbulence, and different options for representing the biophysical controls on transpiration
Snow	One-layer energy–mass balance model that simulates snow accumulation, sublimation, melting, and heat exchange at the snow–atmosphere and snow–soil interfaces	Three-layer energy–mass balance model that represents percolation, retention, and refreezing of meltwater within the snowpack

not step (iii). There were 32 ensemble members, and lateral boundary conditions were defined by applying the ECMWF Reanalysis Interim (ERA-Interim) model analyses. The model simulation domain for the WRF model is shown as the region within the black line (Figs. 1(a) and 1(b)). The horizontal resolution was 27 km, and the model included 28 vertical layers in the atmosphere, and 4 soil layers. There were 100×105 horizontal grid points, thus implying a model domain of approximately 2700×2800 km^2. The northern part of the study domain is occupied by the Central Siberian Plateau, which is relatively flat, whereas the southern part is characterized by mountains and complex topography.

2.2 Ensemble initial conditions

The initial conditions for ensemble prediction were based on the ensemble initiation scheme used in the MLEF (e.g., Suzuki et al., 2017) with some modifications. To obtain an equilibrium state for the initial conditions, we used eight months of spin-up from 00:00 UTC on 1 July 2012 to 00:00 UTC on 3 March 2013 in both the Noah and Noah-MP LSMs. The initial state at 00:00 UTC on 1 July 2013 and the boundary conditions were given by the ERA-Interim global reanalysis dataset (Dee et al., 2011). The approach involves running a single deterministic prediction centered on the initial time of data assimilation (i.e., from time $t = -T$ to $t = T$), where t denotes time and $t = 0$ is the initial time of the ensemble prediction. Here, we used T= 48 hours. The initial uncertainty is defined using time-shifted prediction differences: given a prediction integration of length $2T$, we define an ensemble perturbation using a difference $x_i - x^C$, where x is a state vector, the prediction output time is $\{t_i : -T \leqslant t_i \leqslant T, (i = 1,...,N)\}$, and N is the desired number of ensembles. Index i denotes ensemble member [i.e., $x_i = x(t_i)$], and $x^C = x(0)$ denotes the central prediction at time $t = 0$. The i-th uncertainty vector is given as $p_i = \frac{1}{\sqrt{N}}(x_i - x^C)$. The analysis at $t = 0$ is created by interpolating from the global model as this process produces a better representation of the truth than the prediction that was started 48 hours earlier. Therefore, the initial ensemble perturbations are re-centered around the analysis, where x^A represents the analysis, and the initial conditions (IC) for the ensemble prediction are $x_i^{IC} = x^A + p_i$. Figure 2 shows a schematic

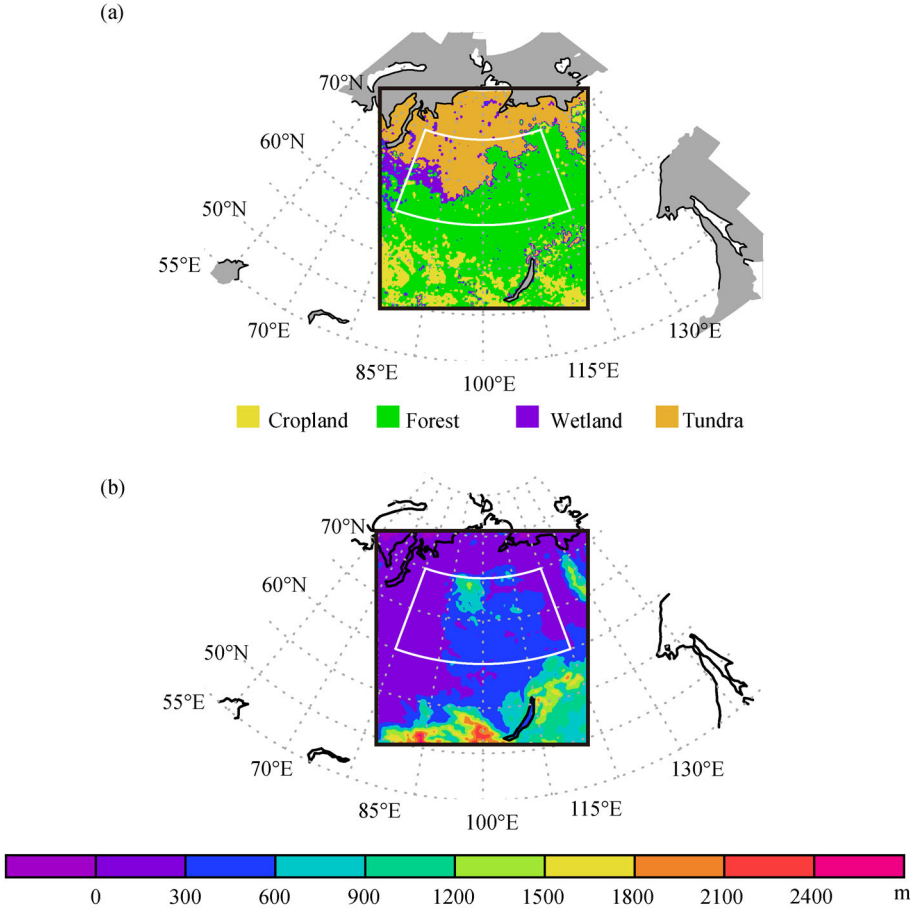

Fig. 1 (a) Map of major vegetation categories, and (b) elevation in the model simulation domain. The regions within the white and the black lines denote the target analysis region (TAR) and the model simulation domain, respectively.

of the procedure used to calculate the initial conditions for the ensemble prediction for each LSM. A deterministic prediction from $t = -T$ to $t = T$ is calculated using both the Noah LSM and the Noah-MP LSM, and $N + 1$ outputs are created ($x_1,\ldots,x_N$ and x^C), where N is the number of ensembles. The initial conditions at $t = -T$ are created from an 8-month spin-up using the Noah and Noah-MP LSMs. The initial uncertainty at $t = 0$ is defined as $p_i = x_i - x^C$. The analysis at $t = 0$ is created by interpolating from the global model. The central time $t = 0$ defines the initial time conditions.

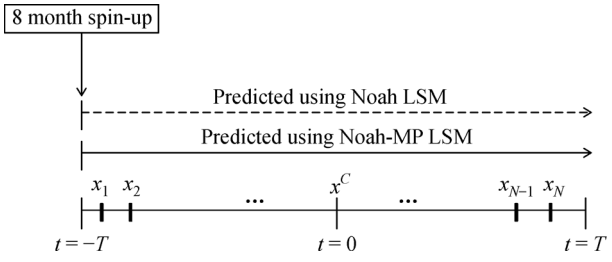

Fig. 2 Initial conditions and their uncertainty values. Central time $t = 0$ defines the initial time conditions. A deterministic prediction from $t = -T$ to $t = T$ is calculated using the (a) Noah LSM and (b) the Noah-MP LSM, and $N + 1$ outputs are created ($x_1,\ldots,x_N$ and x^C), where N is the number of ensembles. The initial conditions at $t = -T$ are created from an 8-month spin-up using the Noah and Noah-MP LSMs as shown in Table 2. The initial uncertainty at $t = 0$ is defined as $p_i = x_i - x^C$. The analysis at $t = 0$ is created by interpolating from the global model.

2.3 Case study

The study area was centered over Siberia, where snow and freezing soils are important components of the natural environment (Suzuki et al., 2006b, 2015b). Figure 1(a) shows the vegetation map used in the LSMs and the synoptic pattern (wind vectors at 500 hPa) obtained from the European Centre for Medium-Range Weather Forecasts (ECMWF) ERA-Interim dataset, which contains global atmospheric reanalysis data. The vegetation categories are summarized in Table 3. The target analysis region (TAR) is encompassed by the white line. Figure 1(b) shows a topographic map of the simulation area. As shown in Fig. 1(a), the TAR is predominantly covered by forest, whereas the northwestern regions are covered by tundra and wetlands. The region consists of flat terrain known as the Siberian Plateau (Fig. 1(b)). Figure 3(a) shows the daily precipitation for 5 March 2013 obtained by the Global Precipitation Climatology Project (GPCP) 1-Degree Daily Precipitation (Version 1.2) (Huffman et al., 2001). The study area was affected by snow precipitation, but nearly half of the TAR was free of precipitation. The Canadian Meteorological Centre (CMC) snow depth (Brasnett, 1999) data for 5 March 2013 reveal that the eastern and northern parts of the TAR had snow depths of 30–40 cm, and that the southwestern part had more than double that depth of snow (Fig. 3(b)).

Table 3 Major and model vegetation categories and surface albedo

Major vegetation category	Model vegetation category	Albedo
Urban	Urban and Built-Up Land	0.15
Cropland	Dryland Cropland and Pasture	0.19
	Irrigated Cropland and Pasture	0.15
	Mixed Dryland/Irrigated Cropland and Pasture	0.17
	Cropland/Grassland Mosaic	0.19
	Cropland/Woodland Mosaic	0.19
	Grassland	0.19
	Shrubland	0.25
	Mixed Shrubland/Grassland	0.23
	Savanna	0.20
Forest	Deciduous Broadleaf Forest	0.12
	Deciduous Needleleaf Forest	0.11
	Evergreen Broadleaf Forest	0.11
	Evergreen Needleleaf Forest	0.10
	Mixed Forest	0.12
Wetland	Water Bodies	0.19
	Herbaceous Wetland	0.12
	Wooded Wetland	0.12
	Barren and Sparsely Vegetated	0.12
Tundra	Herbaceous Tundra	0.16
	Wooded Tundra	0.16
	Mixed Tundra	0.16
	Bare Ground Tundra	0.17
Snow	Snow or Ice	0.70

The initial conditions at 00:00 UTC on 5 March 2013 are shown in Figs. 4(a)–4(d). The Noah LSM determined a significantly lower surface albedo value (0.27 m) than the Noah-MP LSM (0.40 m). This difference can be explained by the vegetation canopy treatment of the Noah-MP, which has an independent canopy energy balance model that should provide more realistic predictions than the Noah LSM. Similarly, the surface temperature from both LSMs showed clear latitudinal differences, whereby the surface temperature determined by the Noah-MP was higher than that of the Noah LSM owing to the lower albedo determined by the Noah-MP. For the Noah LSM, the area-averaged albedo and surface temperature at 00:00 UTC on 5 March 2013 were approximately 0.62 and −35.6°C, respectively, whereas the albedo and surface temperature for the Noah-MP LSM were approximately 0.42 and −32.6°C, respectively.

2.4 Prediction error and uncertainty evaluation

To evaluate the 24-hour prediction error, we used

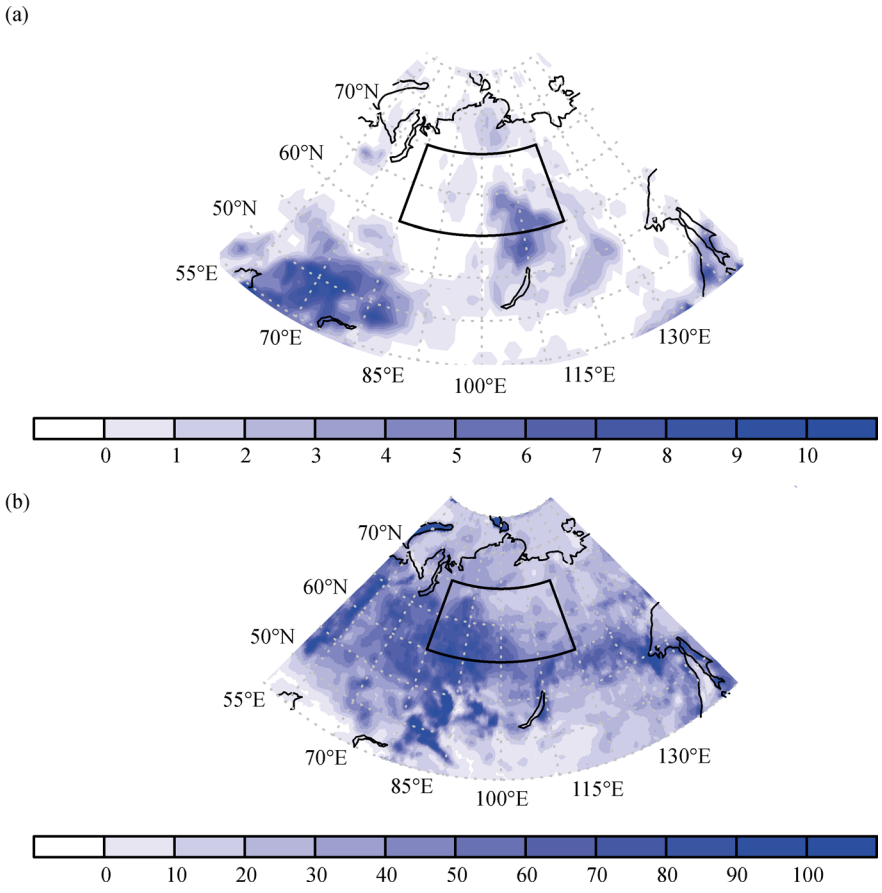

Fig. 3 Spatial distribution of (a) daily precipitation and (b) snow depth on 5 March 2013. The region within the black line denotes the target analysis region (TAR).

observation-based products, denoted by X_O, including GPCP 1-degree daily precipitation, CMC 25 km daily snow depth, and the ERA-Interim reanalysis dataset (approximately 80 km for temperature profiles). Therefore, X_O can also be interpreted as a validation analysis. We evaluated the 24-hour prediction (X_F) against X_O using the root square error (RSE)

$$\mathrm{RSE} = \sqrt{(X_F - X_O)^2}, \tag{1}$$

where X_F is the 24-hour prediction value and X_O is the observational value. Note that this error measure is equivalent to the absolute error $|X_F - X_O|$. Because a control deterministic prediction (X_F) is equivalent to an ensemble mean prediction from a typical ensemble data assimilation process in the MLEF framework, the RSE can also be interpreted as the root-mean-square distance between the analyzed and predicted fields (e.g., Whitaker and Loughe, 1998). Hereafter, we use the RSE as a measure of prediction skill. The ensemble prediction uncertainty is measured by the standard deviation of the prediction error covariance (in our notation), calculated as follows:

$$\sigma = \sqrt{\frac{1}{N}\sum_{i=1}^{N} p_i^2}, \tag{2}$$

where p_i is the i^{th} column of the square root ensemble prediction error covariance.

In addition, when examining the correlation between the prediction error and the uncertainty of that error (which is important because the uncertainty should reflect the true predictability of a variable represented by the prediction error), a large uncertainty indicates a less predictable event, and vice versa. Because low numbers of predictable events are generally more difficult to predict, they should have a larger error; therefore, the prediction error standard deviation and RSE should be positively correlated, which is often termed the spread–skill relationship (Whitaker and Loughe, 1998; Roulston, 2005; Grimit and Mass, 2007). The correlation ρ between the uncertainty and error is often used to check whether the uncertainty is realistic. This correlation is computed by the following:

$$\rho = \frac{X^{\mathrm{T}} Y}{\|X\| \cdot \|Y\|}, \tag{3}$$

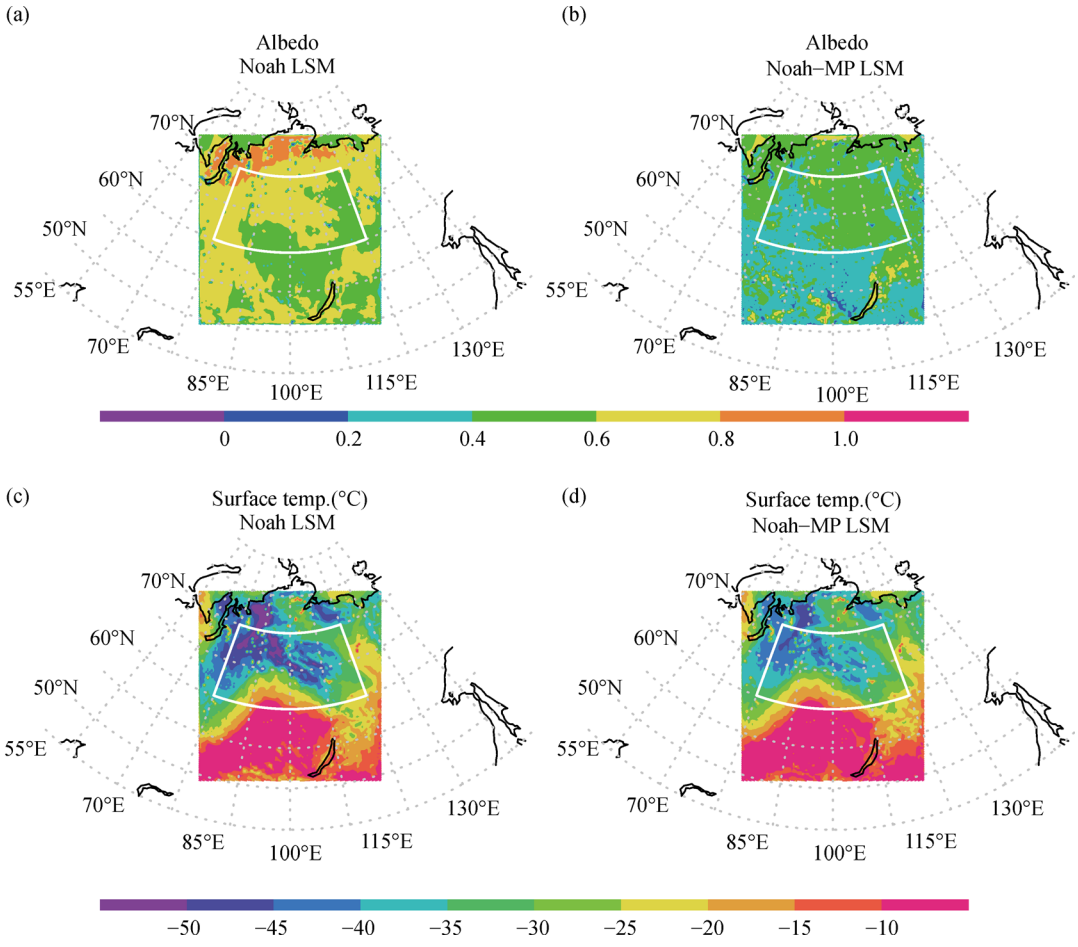

Fig. 4 Maps of the initial state of surface albedo and surface temperature at 00:00 UTC on 5 March 2013 determined by the (a,c) Noah LSM and (b,d) the Noah-MP LSM within the model simulation domain. The region within the white line denotes the target analysis region (TAR).

where X and Y represent the RSE and standard deviation vectors, respectively, and superscript T denotes a transpose. A correlation > 0.5 is generally accepted as satisfactory (e.g., Du, 2007) for establishing that the estimated uncertainty is realistic.

3 Results

3.1 Snow depth prediction

Figures 5(a) and 5(b) show the RSE of snow depth determined by the Noah-MP and Noah LSMs, respectively, at 00:00 UTC on 6 March 2013, which is the end of the 24-hour prediction, using CMC daily snow depth data as a validation. The Noah LSM poorly estimated snow depth compared to the Noah-MP LSM, indicated by significantly larger area-averaged RSE of snow depth (39.1 cm versus 11.0 cm, respectively). By contrast, we do not observe such a significant difference in the snow water equivalent between the Noah and Noah-MP LSMs (115.1 mm and 113.8 mm, respectively). As described in section 2.1, the Noah-MP has multiple snow layers, whereas the Noah LSM has a single snow layer. Thus, the Noah LSM employs the same snow density for the entire snow depth. However, in reality, snow behaves differently because natural snow will be compacted by its own weight, and snow density can therefore increase with depth from the snow surface. The Noah-MP LSM has three snow layers that can replicate a snow density profile similar to that of natural conditions; therefore, the Noah-MP LSM reproduces snow depth better than the Noah LSM.

3.2 Uncertainty in solid precipitation

Figures 6(a) and 6(b) show the RMSE of solid precipitation for the Noah-MP and Noah LSMs, respectively. The Noah-MP LSM showed lower uncertainty than the Noah LSM in the lower-central region of the study area. However, at the southern boundary of central Siberia and in some eastern regions, the RSE for the Noah-MP LSM

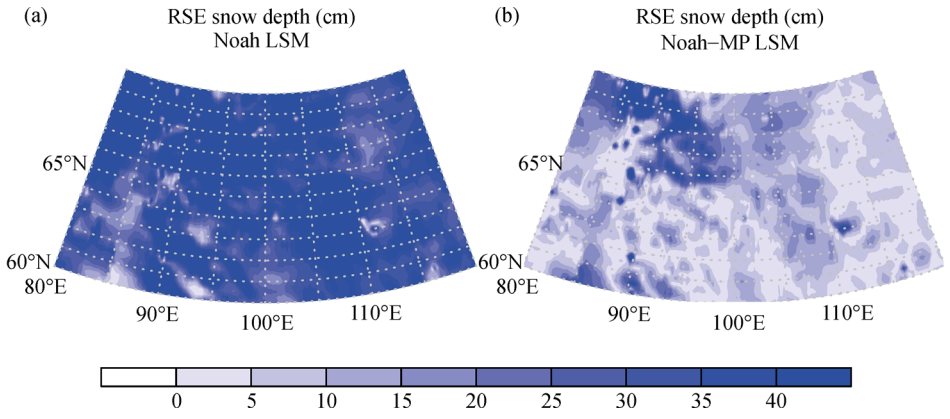

Fig. 5 Maps of the root square error (RSE) of snow depth distribution at 00:00 UTC on 6 March 2013 predicted by the (a) Noah LSM and (b) Noah-MP LSM.

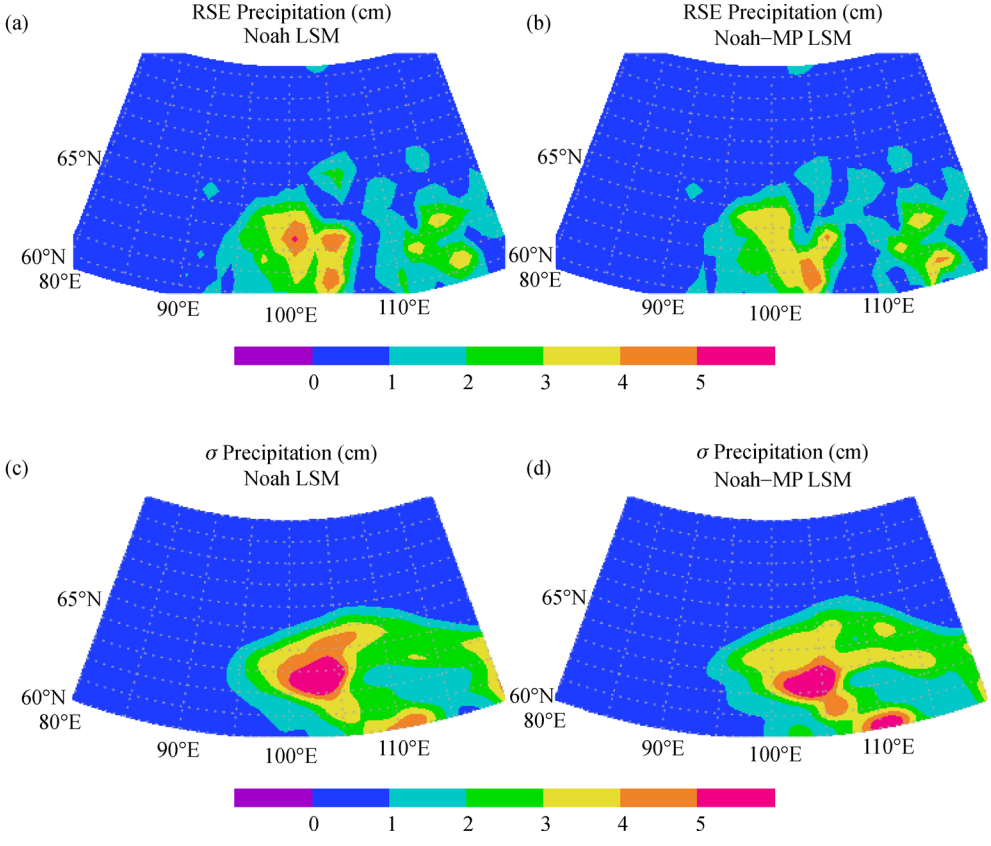

Fig. 6 Maps of root square error (RSE) in precipitation between observation and prediction using (a) Noah and (b) Noah-MP LSMs, and the uncertainty σ in precipitation for the (c) Noah and (d) Noah-MP LSMs at 00:00 UTC on 6 March 2013.

was higher. The TAR-averaged RSE values for the Noah and Noah-MP LSMs were 1.0 mm and 1.1 mm, respectively; thus, the Noah-MP LSM does not provide any clear improvement in the RSE of 24-hour solid precipitation prediction. To address uncertainty, we also show the σ value for the solid precipitation predictions from the two LSMs in Figs. 6(c) and 6(d). The correlation ρ between RSE and σ for the same LSM was 0.67 for the Noah LSM and 0.60 for the Noah-MP LSM. Both of these values suggest that the skill–spread relationships are satisfactory (i.e., > 0.5). In addition, there was almost no difference between the TAR-averaged σ values for the Noah (0.9 mm) and Noah-MP (0.8 mm) LSMs. The magnitudes of both RSE and σ were similar for both LSMs; therefore, we conclude that the uncertainty estimation using both models is realistic.

The comparison of the solid precipitation uncertainties in Figs. 6(c) and 6(d) suggests that the Noah-MP LSM produced somewhat lower uncertainty, especially near the center of the domain, and an area of strong uncertainty in solid precipitation was located south of that in the Noah LSM. Although we could not find any difference in the TAR-averaged solid precipitation uncertainty between the Noah and Noah-MP LSMs in Figs. 6(c) and 6(d), the high-RSE values in Figs. 6(b) and 6(d) (red or orange areas) were lower than those in Figs. 6(a) and 6(c).

3.3 Uncertainty in snow depth change

Next, rather than estimating snow depth itself, we evaluated the uncertainty in daily snow depth change, because snow depth prediction is influenced by the spin-up conditions rather than the 24-hour prediction, as shown in Figs. 5(a) and 5(b). Here, we use the daily observed snow depth change (5–6 March 2013) in CMC snow depth and the model-predicted snow depth change (00:00 UTC 5 March 2013 to 00:00 UTC 6 March 2013) in the Noah and Noah-MP LSMs.

We first test the spread–skill relationship. Figures 7(a)–7(d) show the spatial patterns of the RSE and σ values of daily snow depth change for the Noah and Noah-MP LSMs. We observe some reduction in the RSE in the Noah-MP LSM. The TAR area-averaged RSE values for the Noah and Noah-MP LSMs were 1.8 cm and 1.4 cm, respectively, which are very similar to those of the TAR area-averaged σ for both LSMs (1.5 cm for Noah LSM, 1.1 cm for Noah-MP LSM). Both LSMs gave large RSEs at locations similar to those with highly uncertain solid precipitation predictions, as shown in Figs. 6(c) and 6(d). The correlation ρ between the RSE of snow depth and the σ of solid precipitation was 0.76 for the Noah LSM and 0.76 for the Noah-MP LSM. These correlations are even higher than those for solid precipitation, suggesting that the uncertainty in snow depth change is realistic.

Figures 7(c) and 7(d) show that the Noah-MP LSM estimates include less uncertainty than those of the Noah LSM in the area where solid precipitation occurred, as shown in Fig. 2(a). Furthermore, this area was mostly covered by deciduous needle leaf forest, as shown in Fig. 1(a). The forest canopy in the Noah-MP LSM was separated from the ground surface, whereas the Noah LSM merged the canopy and ground snow; therefore, we attribute the reduced uncertainty in the Noah-MP LSM to its more realistic treatment of the forest canopy. Overall, the comparatively sophisticated Noah-MP LSM can reduce uncertainties related to not only absolute snow

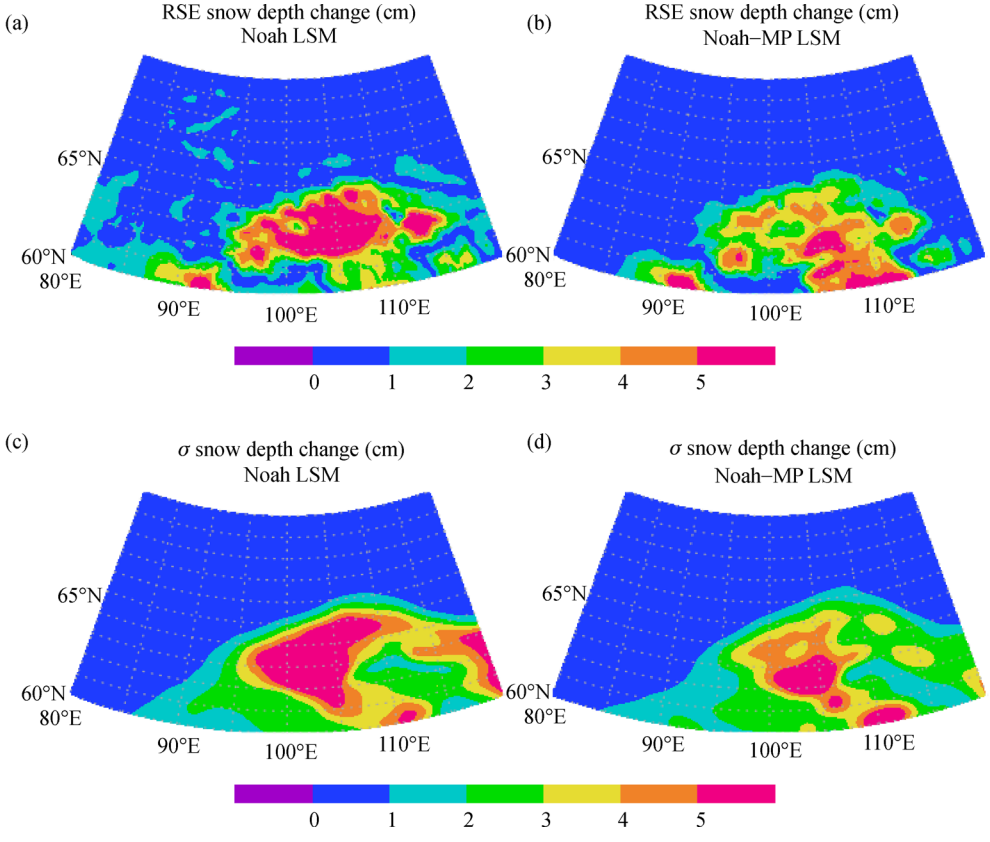

Fig. 7 Maps of the root square error (RSE) of daily snow depth change between observations and predictions using (a) Noah and (b) Noah-MP LSMs, and the uncertainty σ in daily snow depth change for the (c) Noah and (d) Noah-MP LSMs at 00:00 UTC on 6 March 2013.

depth but also daily snow depth change during the 24-hour prediction period. We assume that this result is also due to the use of multiple snow layers and the more realistic forest canopy treatment in the model; that is, the Noah-MP can more accurately calculate the snow density of multiple layers, and the water and energy balance above the forest canopy. We also checked the uncertainty in other surface variables (figures not shown) and found that the more sophisticated LSM can generally reduce uncertainty in land surface parameters.

3.4 Vertical uncertainty changes due to LSMs

Finally, we show how different LSMs affect the uncertainty in air temperature. Figures 8(a)–8(d) show the latitudinally averaged (60°N–70°N) temperature difference (the Noah LSM minus the Noah-MP LSM) for atmospheres of 500 hPa and 850 hPa, at a height of 2 m, and at the surface. Positive values denote improvements in temperature uncertainty determined by the Noah-MP LSM, because such values indicate that the RSE or uncertainty of the Noah-MP LSM was smaller than that of the Noah LSM. The correlation coefficients ρ between the differences (Noah LSM minus Noah-MP LSM) in RSE and σ are 0.39 at the surface, 0.32 at 2 m, 0.42 at 850 hPa, and –0.68 at 500 hPa. Although these correlations between the RSE and σ are not large, the averaged differences in RSE and σ between the two LSMs over the region were very similar: the Noah-MP LSM improved the RSE and σ for surface temperature by 1.7°C and 1.1°C, for 2-m temperature by 0.6°C and 0.4°C, for 850-hPa temperature by 0.3°C and 0.0°C, and for 500-hPa temperature by –0.2°C and 0.1°C, respectively. The negative correlation at 500 hPa results from the negative difference in RSE between the Noah and Noah-MP LSMs. Small differences in uncertainty are observed in the lower (850 hPa) and middle (500 hPa) atmosphere. However, near the surface (at 2 m and at the surface), the uncertainty differences are much more positive, suggesting that the Noah LSM produces larger uncertainty than the Noah-MP LSM. As anticipated, the effect of the LSM is confined to the near-surface layers of the atmosphere.

4 Discussion

Table 4 presents a summary of the results. Accordingly, the more sophisticated Noah-MP LSM snow model, which includes multiple snow layers, can reduce the error in snow depth predictions by simulating realistic snow density profiles within the modeled snow layers. Cai et al. (2014) showed that the Noah-MP provided the best simulation of annual terrestrial water storage throughout the US, relative to Noah LSM. Our snow depth predictions are directly related to terrestrial water storage because snow is a major component of annual terrestrial water. Thus, we conclude that the Noah-MP LSM can provide more realistic snow simulation than Noah LSM. In terms of predicting solid precipitation, sophisticated LSMs do not contribute to reducing TAR-averaged solid precipitation errors but could

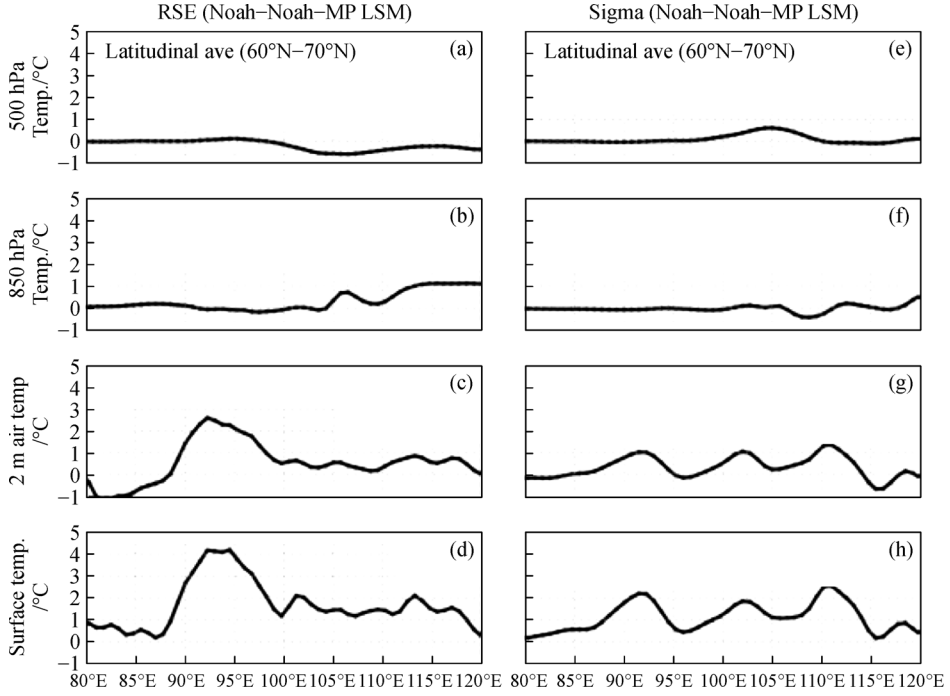

Fig. 8 Latitudinally averaged (60°N–70°N) zonal cross-section of root square error (RSE) and uncertainty σ in temperature at each vertical level for (a, e) 500 hPa, (b, f) 850 hPa, (c, g) 2 m air temperature, and (d, h) surface temperature.

Table 4 Summary of prediction skill for the Noah-MP LSM, compared with Noah LSM results

Parameters	Difference in area-averaged RSE (Noah LSM minus Noah-MP LSM)	Results
Snow depth/cm	13	Significantly improved
Solid precipitation/mm	0.1	Improved locally, but no area-averaged improvement
Surface temperature/°C	1.7	Improved
2-m air temperature/°C	0.6	Improved
850-hPa temperature/°C	0.3	Slightly improved
500-hPa temperature/°C	−0.2	Not improved

reduce local prediction errors. In addition, these results suggest that a sophisticated LSM can reduce the uncertainty in near-surface layers, which may be why sophisticated LSMs such as Noah-MP do not improve the uncertainty in solid precipitation predictions, as these LSMs have almost no effect on temperature or cloud hydrometeors for most parts of the atmospheric temperature in the context of short-range weather prediction. These results are consistent with those of Orth et al. (2016), who implied that these sophisticated models would have no impact on precipitation or temperature predictions because their reduced uncertainty might lead to an increased compensating error. On the other hand, Hu et al. (2014) demonstrated that, in WRF simulations, Noah-MP LSM performed slightly better (i.e., better predicted the precipitation field) than Noah LSM in reproducing severe drought events in Southwest China. Although we did not find any differences in area-averaged solid precipitation between Noah and Noah-MP LSMs, the WRF simulation with Noah-MP LSM locally improved solid precipitation prediction, especially in areas with heavy snowfall, which supports the findings of Hu et al. (2014).

Finally, we discuss the limitations of the present result. We focused on solid precipitation and snow depth predictions over a 24-hour period. Douville (2010) showed that land surface hydrology enabled reliable seasonal forecasting of surface air temperature and precipitation predictability over Eurasia. Compared with such seasonal evaluations, the 24-hour time frame employed here is a very short period over which to compare the solid precipitation predictions between two LSMs. Despite these constraints, we showed some positive impacts for 24-hour weather prediction resulting from more sophisticated land surface models such as Noah-MP LSM. Further improvements in predictions require the use of a global climate model such as a general circulation model, because regional forecasts can be limited by the lateral boundary conditions given by a global model, and the effective prediction time-scale is strongly dependent on boundary conditions and the size of the calculation domain.

Overall, the differences in results between the two LSMs analyzed in this study can be largely explained by the reduction of uncertainty achieved when using the sophisticated land surface model, which in turn improved weather prediction.

5 Conclusions

We investigated the uncertainty in solid precipitation and snow depth prediction, as well as the change in uncertainty in atmospheric temperature, using two different LSMs. Our findings were as follows.

1) For the same LSM, the RSE and of snow precipitation show highly positive correlation (>0.5), indicating that the uncertainty estimation is realistic.

2) The inclusion of multiple snow layers in the Noah-MP model is beneficial for reducing snow depth uncertainty.

3) The uncertainties in daily snow depth change were reduced more in the Noah-MP than in the Noah model, but the uncertainty in daily solid precipitation showed minimal difference between the two LSMs.

4) According to a vertical cross-section of the latitudinally averaged atmospheric temperature uncertainty, the more sophisticated LSM mainly improved temperature uncertainty within the surface layer, whereas the lower and middle atmosphere were not strongly affected by either LSM. However, the uncertainty reduction was much greater for Noah-MP than for the Noah LSM.

5) The more sophisticated Noah-MP LSM achieves a greater reduction in uncertainty, which supports the prevailing belief (e.g., Du, 2007) that using prediction models with improved skill provides improved predictability and reduced uncertainty in prediction.

Acknowledgements We thank Prof. Steven R. Fassnacht and two anonymous reviewers for their contributions to improving the first draft of this article. We declare no conflicts of interest and no financial disclosure. Parts of this study were supported by a Grant-in-Aid for Scientific Research (C) (No. 16K00581), and a Grant-in-Aid for Challenging Exploratory Research (No. 25550022). The second author acknowledges partial support from the Office of Naval Research under contract N000149169192040.

References

Brasnett B (1999). A global analysis of snow depth for numerical weather prediction. J Appl Meteorol, 38(6): 726–740

Cai X, Yang Z-L, Xia Y, Huang M, Wei H, Leung L R, Ek M B (2014). Assessment of simulated water balance from Noah, Noah-MP, CLM, and VIC over CONUS using the NLDAS test bed. Journal of Geophysical Research: Atmospheres, 119(13): 13751–13770

Chou M D, Suarez M J (1999). A solar radiation parameterization for atmospheric studies. NASA/TM-1999-104606/VOL15. NASA Technical Report. Greenbelt, MD: Goddard Space Flight Center

Dee D P, Uppala S M, Simmons A J, Berrisford P, Poli P, Kobayashi S, Andrae U, Balmaseda M A, Balsamo G, Bauer P, Bechtold P, Beljaars A C M, van de Berg L, Bidlot J, Bormann N, Delsol C, Dragani R, Fuentes M, Geer A J, Haimberger L, Healy S B, Hersbach H, Hólm E V, Isaksen L, Kållberg P, Köhler M, Matricardi M, McNally A P, Monge-Sanz B M, Morcrette J J, Park B K, Peubey C, de Rosnay P, Tavolato C, Thépaut J N, Vitart F (2011). The ERA-Interim reanalysis: configuration and performance of the data assimilation system. Q J R Meteorol Soc, 137(656): 553–597

Douville H (2010). Relative contribution of soil moisture and snow mass to seasonal climate predictability: a pilot study. Clim Dyn, 34(6): 797–818

Du J (2007). Uncertainty and ensemble forecast. National Weather Service, Office of Science & Technology, Science & Technology Infusion Lecture Series, 42 pp

Ek M B (2003). Implementation of Noah land surface model advances in the National Centers for Environmental Prediction operational mesoscale Eta model. J Geophys Res, 108(D22): 8851

Grimit E P, Mass C F (2007). Measuring the ensemble spread-error relationship with a probabilistic approach: Stochastic ensemble results. Mon Weather Rev, 135(1): 203–221

Hong S Y, Noh Y, Dudhia J (2006). A new vertical diffusion package with an explicit treatment of entrainment processes. Mon Weather Rev, 134(9): 2318–2341

Hu Z H, Xu Z F, Zhou N F, Ma Z G, Li G P(2014). Evaluation of the WRF model with different land surface schemes: a drought event simulation in southwest China during 2009–10. Atmos Ocean Sci Lett, 7(2): 168–173

Huffman G J, Adler R F, Morrissey M M, Bolvin D T, Curtis S, Joyce R, McGavock B, Susskind J (2001). Global precipitation at one-degree daily resolution from multisatellite observations. J Hydrometeorol, 2 (1): 36–50

Iacono M J, Delamere J S, Mlawer E J, Shephard M W, Clough S A, Collins W D (2008). Radiative forcing by long-lived greenhouse gases: calculations with the AER radiative transfer models. J Geophys Res, 113(D13): D13103

Jin J, Miller N L, Schlegel N (2010). Sensitivity study of four land surface schemes in the WRF model. Adv Meteorol, 2010: 1–11

Kain J S (2004). The Kain–Fritsch convective parameterization: an update. J Appl Meteorol, 43(1): 170–181

Lin Y L, Farley R D, Orville H D (1983). Bulk parameterization of the snow field in a cloud model. J Clim Appl Meteorol, 22(6): 1065–1092

Mahrt L, Ek M (1984). The influence of atmospheric stability on potential evaporation. J Clim Appl Meteorol, 23(2): 222–234

Niu G Y, Yang Z L, Mitchell K E, Chen F, Ek M B, Barlage M, Kumar A, Manning K, Niyogi D, Rosero E, Tewari M, Xia Y (2011). The community Noah land surface model with multiparameterization options (Noah-MP): 1. Model description and evaluation with local-scale measurements. J Geophys Res, 116(D12): 12109

Orth R, Dutra E, Pappenberger F (2016). Improving weather predictability by including land surface model parameter uncertainty. Mon Weather Rev, 144(4): 1551–1569

Roulston M S (2005). A comparison of predictors of the error of weather forecasts. Nonlinear Process Geophys, 12(6): 1021–1032

Skamarock W C, Klemp J B, Dudhia J, Gill D O (2008). A description of the advanced research WRF Version 3. NCAR Technical note-475 + STR, 113 pp

Suzuki K, Kodama Y, Nakai T, Liston G E, Yamamoto K, Ohata T, Ishii Y, Sumida A, Hara T, Ohta T (2011). Impact of land-use changes on snow in a forested region with heavy snowfall in Hokkaido, Japan. Hydrol Sci J, 56(3): 443–467

Suzuki K, Konohira E, Yamazaki Y, Kubota J, Ohata T, Vuglinsky V (2006a). Transport of organic carbon from the Mogot Experimental Watershed in the southern mountainous taiga of eastern Siberia. Nord Hydrol, 37(3): 303–312

Suzuki K, Kubota J, Ohata T, Vuglinsky V (2006b). Influence of snow ablation and frozen ground on spring runoff generation in the Mogot Experimental Watershed, southern mountainous taiga of eastern Siberia. Hydrol Res, 37: 21–29

Suzuki K, Liston G E, Kodama Y (2015a). Variations of winter surface net shortwave radiation caused by land-use change in northern Hokkaido, Japan. J For Res, 20(2): 281–292

Suzuki K, Liston G E, Matsuo K (2015b). Estimation of continental-basin-scale sublimation in the Lena River basin, Siberia. Adv Meteorol, 2015: 1–14

Suzuki K, Matsuo K, Hiyama T (2016). Satellite gravimetry-based analysis of terrestrial water storage and its relationship with run-off from the Lena River in eastern Siberia. Int J Remote Sens, 37(10): 2198–2210

Suzuki K, Zupanski M, Zupanski D (2017). A case study involving single observation experiments performed over snowy Siberia using a coupled atmosphere-land modelling system. Atmos Sci Lett, 18(3): 106–111

Whitaker J S, Loughe A F (1998). The relationship between ensemble spread and ensemble mean skill. Mon Weather Rev, 126(12): 3292–3302

Yu M, Wang G, Chen H (2016). Quantifying the impacts of land surface schemes and dynamic vegetation on the model dependency of projected changes in surface energy and water budgets. J Adv Model Earth Syst, 8(1): 370–386

Zeng X M, Wang N, Wang Y, Zheng Y, Zhou Z, Wang G, Chen C, Liu H (2015). WRF-simulated sensitivity to land surface schemes in short and medium ranges for a high-temperature event in East China: a comparative study. J Adv Model Earth Syst, 7(3): 1305–1325

Zupanski M (2005). Maximum likelihood ensemble filter: theoretical aspects. Mon Weather Rev, 133(6): 1710–1726